DOI: 10.15480/882.9300

Eighth International Symposium on Marine Propulsors
smp'24, Berlin, Germany, March 2024

Improving Accuracy of Panel Method under Low Advance Ratio Conditions

Jinghan Su[1], Yongle Ding[2], Youjiang Wang[1], Jian Li[2]

[1]Shanghai Jiao Tong University, Shanghai, China
[2]Xi'an Precision Machinery Research Institute, Xi'an, China

ABSTRACT

As a pivotal technique in the optimization of marine propellers, the panel method is frequently employed for handling a substantial volume of propeller designs due to its simplicity and rapid computational capabilities. However, it is widely acknowledged that the panel method can introduce significant torque errors, particularly under low advance ratio conditions. One of the contributing factors to this error is the panel method's incapacity to adequately simulate the generation of leading-edge vortices during the propeller's rotation. A leading-edge vortex correction model has been devised to alleviate the computational errors induced by the panel method, albeit without extensive validation. In this study, a comparative analysis of the results obtained from the RANS method and the panel method, corrected using the leading-edge vortex model, has been conducted. The comparison reveals a substantial resemblance in the surface pressure distribution between the two approaches. This discovery further underscores the reliability of the proposed leading-edge vortex correction model. Through computational investigations, it becomes evidently clear that this correction model effectively reduces torque calculation errors.

Keywords

Panel Method; Leading-edge Vortex; Low Advance Ratios; Torque error; Numerical Simulation

1 INTRODUCTION

As the economic development and living standards improve, there is a concomitant increase in energy demand. Fossil fuels currently constitute a pivotal energy source with extensive applications, ranging from automotive and industrial fuels to raw materials for plastics and cosmetics. Nevertheless, the large-scale utilization of fossil fuels engenders greenhouse gas emissions, notably carbon dioxide, exacerbating global warming and precipitating environmental issues such as rising sea levels, glacial melt, and ocean acidification (Mogollon et al 2022). These issues confer irreversible damage upon both human society and the natural environment. Globalization has propelled international trade, with maritime shipping playing a critical role in economic progress. Encompassing two-thirds of the Earth's surface, the majority of global cargo transportation is carried out through maritime shipping (Majumder & Maity 2023). Maritime shipping, driven by high carrying capacity, cost-effectiveness, and safety, stands as an economic pillar. Yet, despite its advantages, maritime transport emits nitrogen oxides, sulfur dioxide, particulate matter, and greenhouse gases during vessel operations, leading to marine pollution and environmental destruction. Gradually, maritime transport has emerged as a primary contributor to global warming. To mitigate these effects, international organizations and governments seek sustainable approaches, propelling innovations within the maritime industry to reduce its environmental burden. In 2021, the International Maritime Organization introduced amendments to Annex VI of the International Convention for the Prevention of Pollution from Ships (Wang 2022). The aim was to establish tools such as EEXI and CII to foster the sustainable development of the maritime shipping sector.

Propeller energy-saving technologies have garnered significant attention within the domain of maritime energy conservation, impacting energy consumption and environmental concerns. The current dominant method for optimizing propeller designs is via Computational Fluid Dynamics (CFD). Numerous research institutions and enterprises are leveraging CFD technology to enhance propeller efficiency and reduce energy consumption in maritime vessels. While traditional CFD methods primarily employ RANS approaches, the complex nature of turbulence models and grid generation means a long computation time. In contrast to traditional RANS methods, the Panel Method offers certain advantages in terms of simplicity in configuration and rapid computation, particularly in the analysis and optimization of large-scale scenarios.

In 1964, Hess and Smith employed the Panel Method for the first time in the aerospace engineering domain to calculate the potential flow around three-dimensional objects with no lift. With the continuous development of computer technology and numerical computation methods, the application of the panel method has seen ongoing expansion and improvement (Hess & Smith 1964). In 1974, Merino introduced a velocity-potential-based panel method suitable for complex three-dimensional

geometries, building upon the velocity-based panel method. This theory still relies on the source panel method but introduces the concept of a velocity potential in the computation of source strengths, thus enhancing both the accuracy and efficiency of calculations (Morino & Kuo 1974). Building upon this foundation, Webster proposed an improved panel method in 1975, which involved discretizing the object's surface into small triangular panels instead of quadrilateral panels. Compared to quadrilateral panels, triangular panels offer greater flexibility and precision, thereby enhancing computational accuracy. The method has been continuously expanded and improved (Webster 1975). In 1988, Lee introduced the panel method based on potential flow theory and rigid ship hull assumptions, considering the rotational effects of propeller rotation and proposing methods to compute stable flow fields around ship propellers (Lee 1988). In practical engineering applications, this approach can offer more accurate and detailed numerical simulations for the hydrodynamic studies of vessels such as ships and submarines.

Despite its simplicity and quick calculations, the panel method has a problem of low accuracy in simulating propeller hydrodynamics under low advance ratio conditions. Few studies have focused on improving this aspect. This study believes that the main reason for the error under low advance ratio conditions is that the panel method cannot simulate the leading-edge vortex of propeller blades well. The research rechecks a leading-edge vortex model proposed previously (Krüger et al 2019) to reduce the error that occurs in this case.

To enhance the accuracy of the leading-edge vortex correction model, this study initially employs a RANS method to obtain the surface pressure distribution. These surface pressure distributions are then compared with those generated by the leading-edge vortex correction model to validate the simulation performance of the correction model.

2 METHODOLOGY

2.1 Panel Method

The Panel Method is a Computational Fluid Dynamics (CFD) technique primarily employed for solving potential flow problems, such as the flow of incompressible, inviscid fluids around objects. In the Panel Method, the surface of the object is discretized into a series of discrete panels, with each panel having a distribution of source or vortex strength. By satisfying boundary conditions, it becomes possible to solve for the distribution of source or vortex strengths, and subsequently obtain velocity and pressure distributions within the flow field (Wang et al 2022).

In the context of open water performance, the propeller can be regarded as a rotating object submerged in an inflow velocity V. Its velocity potential ϕ can be described using the Laplace equation:

$$\nabla^2\phi = 0 \tag{1}$$

Let $S=S_B+S_W+S_\infty$, where S_B is the surface of the propeller immersed in the fluid, S_W represents the wake surface, and S_∞ denotes the outer boundary in the far-field. According to Green's theorem, the disturbance potential ϕ at any point P(x, y, z) can be represented by the following integral:

$$E\phi(p) = -\frac{1}{4\pi}\iint_S \left[\phi(Q)\frac{\partial}{\partial n_Q}\left(\frac{1}{R(P,Q)}\right) - \frac{\partial\phi(Q)}{\partial n_Q}\frac{1}{R(P,Q)}\right]dS \tag{2}$$

where R(P, Q) represents the distance between point P and another point Q. When P is inside S_B, E=0; when P is on S_B, E=0.5; when P is outside S_B, E=1.

In simulating the open-water performance of a propeller using the panel method, several boundary conditions are imposed to constrain the solution and ensure the closure of the system of equations. For each point on the propeller surface S_B, it is essential to ensure that the fluid does not flow through the surface, meaning the velocity along the normal direction is zero:

$$\frac{\partial\phi}{\partial n_Q} = -\mathbf{V}\cdot\mathbf{n}_Q \tag{3}$$

where n_Q refers to the unit normal vector on the boundary surface, and V refers to the inflow velocity of the propeller.

Based on the assumption of a zero-thickness vortex sheet, when the fluid passes through the vortex sheet S_W, there are no velocity and pressure jumps in normal direction:

$$\left(\frac{\partial\phi}{\partial n_{Q_0}}\right)^+ - \left(\frac{\partial\phi}{\partial n_{Q_0}}\right)^- = 0 \tag{4}$$

$$p^+ - p^- = 0 \tag{5}$$

where Q_0 is a point on the trailing vortex sheet, and p+ and p- represent the pressures on the upper and lower surfaces of the vortex sheet, respectively.

For the outer boundary surface S_∞, which is far away from the propeller, the flow of fluid on this surface should gradually approach a steady state, meaning that the disturbance potential on this surface should gradually become zero:

$$\frac{\partial\phi}{\partial x}\mathbf{i} + \frac{\partial\phi}{\partial y}\mathbf{j} + \frac{\partial\phi}{\partial z}\mathbf{k} \to 0 \tag{6}$$

The difference between the external potential and the internal potential is defined as the dipole:

$$-\mu = \phi_e - \phi_i \tag{7}$$

Where ϕ_e is the external potential, ϕ_i is the internal potential, and $-\mu$ represents the dipole.

The difference between the normal derivatives of the external potential and the internal potential is defined as the source：

$$-\sigma = \frac{\partial\phi_e}{\partial n} - \frac{\partial\phi_i}{\partial n} \tag{8}$$

where $\partial\phi_e/\partial n$ is the normal derivative of the external potential, $\partial\phi_i/\partial n$ is the normal derivative of the internal potential, and -σ represents the source.

Taking into account the above conditions, equation (2) can be expanded on the surface of the propeller and its wake as follows:

$$\begin{aligned}\phi(P) = \frac{1}{2\pi}\Bigg[&\iint_{S_B}\phi(Q)\frac{\partial}{\partial n_Q}\left(\frac{1}{R(P,Q)}\right)dS + \iint_{S_B}\left(\mathbf{V}\cdot\mathbf{n}_Q\right)\left(\frac{1}{R(P,Q)}\right)dS \\ &+ \iint_{S_W}\Delta\phi(Q_0)\frac{\partial}{\partial n_{Q_0}}\left(\frac{1}{R(P,Q_0)}\right)dS\Bigg]\end{aligned} \tag{9}$$

where the first integral represents a distribution of normal dipoles with a strength of $-\phi(Q)$ on the body surface. It corresponds to a force distributed across the surface of the body, resulting in a potential field. The second integral represents a source distribution with a strength of $-V \cdot n_Q$ on the body surface. This indicates the presence of sources in certain regions of the body surface, creating a source potential field. Lastly, the third integral represents a distribution of normal dipoles with a strength of $-\Delta\phi(Q_0)$ on the vortex sheet.

The trailing vortex is one of the primary mechanisms responsible for generating lift, and it forms at the rear of an object, contributing to the overall lift force. When dealing with lift-related problems, the Pressure Kutta Condition serves as a crucial criterion for simulating and controlling these trailing vortices. The fundamental concept behind the Pressure Kutta Condition is to ensure a smooth transition of pressure at the object's trailing edge, avoiding abrupt pressure changes. Therefore, the Pressure Kutta Condition requires that the pressure gradient on the surface elements at the object's trailing edge should be zero:

$$(\Delta p) = p^{+} - p^{-} = 0 \tag{10}$$

where p+ and p- represent the pressure on the upper and lower surfaces of the trailing vortex sheet, respectively.

In Equation (9), the unknowns are the dipole strengths on the propeller surface (Su et al 2004). By incorporating the pressure Kutta condition, numerical solutions for this integral equation can be obtained (Wang et al 2023).

2.2 RANS Method

Reynolds Averaged Navier-Stokes Simulation (RANS) is one of the most commonly used turbulence simulation methods in current engineering applications. Its core idea involves statistically averaging the mass, momentum, and energy transport equations that reflect flow characteristics, thus establishing turbulence models to close the NS equation system (Ivashchenko et al 2023).

Turbulence models can be categorized into eddy-viscosity models and Reynolds stress models based on their solution approaches. In this study, for simulating the hydrodynamic performance of the propeller, the focus has been on the two-equation models within the SST k-omega model. The SST k-omega turbulence model is a widely used two-equation turbulence model in computational fluid dynamics. It is designed to simulate the behavior of turbulent flows by solving two transport equations, one for the turbulent kinetic energy and the other for the specific dissipation rate.

3 OPEN WATER SIMULATION OF PROPELLER BASED ON THE RANS METHOD

The present section employs the RANS method to conduct simulation and analysis of the hydrodynamic performance of a PPTC propeller. For the PPTC propeller, we refer to advance ratios lower than 0.7 as low advance ratios. Specifically, the simulation is performed at advance ratios of 0.267, 0.4006, and 0.6676, generating sectional pressure coefficient distribution plots for the propeller blade at 0.7R. The outcomes of this work serve as a crucial reference for the subsequent validation of a panel method leading-edge vortex correction model.

3.1 Introduction to the PPTC

The propeller used in this study is the VP1304 propeller from the Potsdam Propeller Test Case (PPTC). Its geometric parameters are shown in Table 1 (Barkmann 2011).

Table 1 Parameters of VP1304 propeller

Property	Unit	Quantity
Diameter	[m]	0.25
Pitch ratio	[-]	1.635
Area ratio	[-]	0.77896
Skew	[°]	18.837
Hub ratio	[-]	0.3
Number of blade	[-]	5

3.2 Creating the Computational Domain Model

In STAR-CCM+, static and rotating domains are created, with the propeller diameter D used to define the dimensions, as depicted in Figure 1. The inlet of the static domain is set at 3D ahead of the propeller, while the outlet is set at 7D behind the propeller, with a radius of 2.5D. The rotating domain is positioned with its front end at a distance of 0.5D ahead of the propeller and its rear end at a distance of 0.5D behind the propeller, with a radius of 0.6D. Additionally, a new cylindrical component with a radius of 0.72D and a height of 7.6D is created, as shown in Figure 2. This cylindrical component is used to refine the mesh around the propeller.

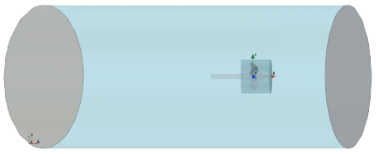

Figure 1 The static and computational domains

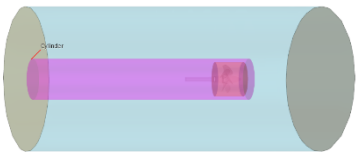

Figure 2 Cylindrical refinement region

3.3 Mesh Generation

The cut-cell mesh generators and prism layer mesh generators are employed to generate the mesh. A target Y+ value of 80 is used to set the parameters for the prism layer mesh. In the automatic mesh default control module, the prism layers are set to five, with a prism layer stretching ratio of 1.2 and a total prism layer thickness of 0.0108D. Fine mesh refinement was applied to the blade surfaces, the interface between the static domain and the rotating domain, and the far field of the static domain. The target surface size for the blade surfaces was set to 0.009D, with a minimum surface size of 0.0018D. The cut-cell mesh generator's surface growth rate was set to "fast". For the

interface between the static domain and the rotating domain, the prism layer had one layer and a total thickness of 0.018D, with boundary overrides applied. In the far field of the static domain, the target surface size was set to 0.576D to reduce grid density and computation time. For the cylindrical component, a volume mesh refinement was performed, and the cut-cell mesh generator was defined with isotropic sizing, set to 0.018D. After refining the surface grids of the propeller blades, the interfaces between the stationary and rotating domains, and the far-field of the stationary domain, a volume grid is generated around the propeller, as shown in Figure 3.

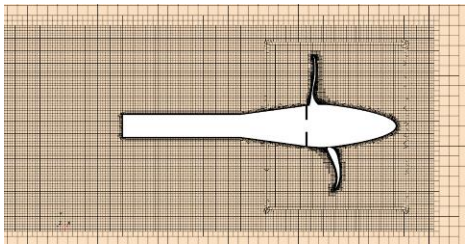

Figure 3 Volume grid around propeller

3.4 Boundary Conditions

In the static domain, the inlet is configured as a velocity inlet, and the outlet is set as a pressure outlet. To mitigate boundary effects, this study defines the surface of the static flow domain as a symmetry plane. The remaining surfaces between the rotating domain and the static domain are designated as internal interfaces.

3.5 Comparison with Experiment Data

The following dimensionless coefficients are used to describe the open-water performance of a propeller.

$$J = \frac{V}{nD} \tag{11}$$

where J represents the advance coefficient, V is the inflow velocity, n is the rotational speed, and D is the propeller diameter.

$$K_T = \frac{T}{\rho n^2 D^4} \tag{12}$$

where K_T denotes the thrust coefficient, T is the thrust force, and ρ is the density of water.

$$K_Q = \frac{Q}{\rho n^2 D^5} \tag{13}$$

where K_Q stands for the torque coefficient, and Q is the torque.

$$\eta_0 = \frac{K_T}{K_Q} \cdot \frac{J}{2\pi} \tag{14}$$

where η_0 represents the open-water efficiency.

In this study, the open-water performance of the propeller is simulated using the SST k-omega model. The comparative analysis between the simulation results and the experimental data is presented in Table 2, while the open-water characteristic curve is illustrated in Figure 4. According to Table 2, the relative errors in the calculation of thrust coefficient, torque coefficient, and open-water efficiency using the SST k-omega model are all less than 4%. This indicates that the computed results are reasonably accurate. Therefore, these results can be utilized for the analysis of the pressure distribution on the propeller surface.

Table 2 Comparison of computation data under SST k-omega model

	J	0.267	0.401	0.668	0.799
K_T	Exp.	0.829	0.744	0.585	0.505
	RANS	0.837	0.758	0.590	0.509
	Rel. Error	0.97%	1.88%	0.85%	0.79%
$10K_Q$	Exp.	1.789	1.616	1.325	1.184
	RANS	1.846	1.682	1.356	1.208
	Rel. Error	3.19%	4.08%	2.34%	2.03%
η_0	Exp.	0.197	0.294	0.469	0.542
	RANS	0.193	0.287	0.462	0.535
	Rel. Error	-2.03%	-2.38%	-1.49%	-1.29%

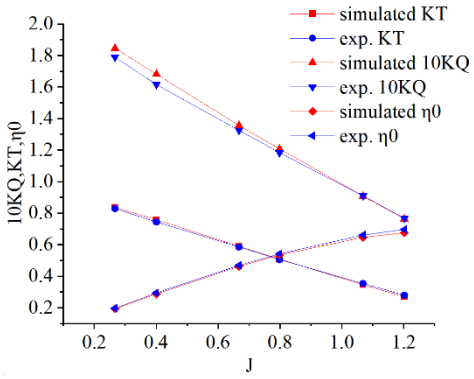

Figure 4 SST k-omega model propeller open water characteristic curve

3.6 Propeller Pressure Distribution

The RANS simulations are used to provide high fidelity data of the propeller's surface pressure distribution. The comparative analysis focuses on the sections at r/R=0.7, where R is the propeller radius, r is the radius at a certain location on the propeller, as depicted in Figure 5.

In Figure 6, the vertical axis C_p represents the pressure coefficient, defined as:

$$C_p = \frac{p}{0.5\rho(V^2 + V_w^2)} \tag{15}$$

where V_w is the tangential velocity at a certain radius while the propeller is rotating; and p is surface pressure.

The horizontal axis x/c represents the dimensionless chordwise position from leading edge to trailing edge of a propeller blade section. x/c=0 denotes the leading edge, and x/c=1 corresponds to the trailing edge.

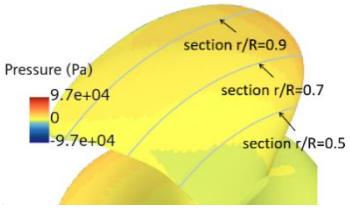

Figure 5 Propeller blade sections

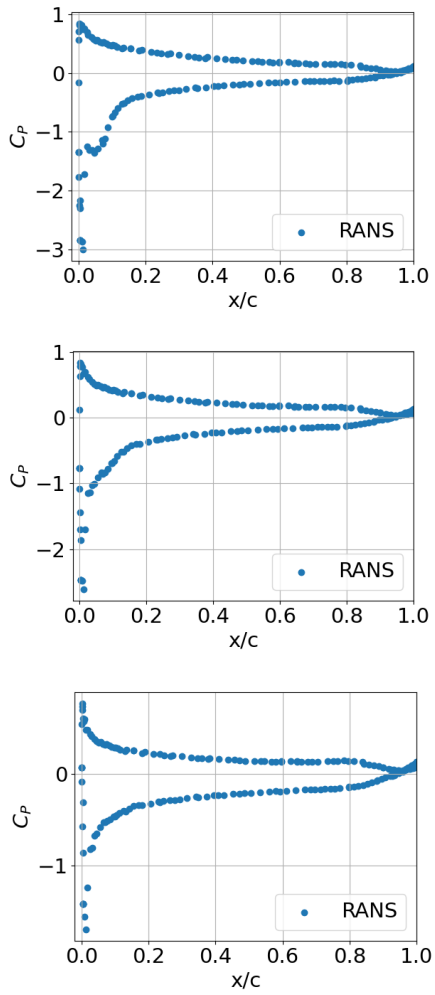

Figure 6 Surface pressure distribution of the propeller blade section at r/R=0.7 obtained with RANS at advance ratios of 0.267, 0.4006, and 0.6676

4 IMPROVED PANEL METHOD MODEL BASED ON LEADING EDGE VORTEX CORRECTION

In this section, a correction model for the leading-edge vortex is proposed based on the mechanism of its generation. A comparative analysis is conducted with the surface pressure distribution from Section 3 to validate the accuracy of the correction model.

4.1 The Comparison of Surface Pressure Distribution Obtained from the Panel Method and the RANS Method

The panel method software potHydro, which is an inhouse potential code for hydrodynamics developed in Prof. Youjiang Wang's group at Shanghai Jiao Tong University, is utilized for propeller open-water performance simulation.

Table 3 gives the results without the leading-edge correction model. It indicates that under low inflow conditions, there is a significant torque error when using the panel method for open water simulations. Figure 7 shows the pressure distributions obtained with the panel method together with those obtained with RANS. It reveals a substantial disparity between the surface pressure distribution obtained by the panel method and the RANS method. The surface pressure distribution obtained by the panel method exhibits a large low-pressure region near the leading edge.

Table 3 Comparison of panel method data without correction

J	Data Type	K_T	$10K_Q$
0.267	Exp.	0.829	1.789
	Panel Method	0.744	1.361
	Rel. Error	-10.533%	-23.924%
0.4006	Exp.	0.744	1.615
	Panel Method	0.675	1.314
	Rel. Error	-9.274%	-18.638%
0.6676	Exp.	0.585	1.325
	Panel Method	0.541	1.185
	Rel. Error	-7.521%	-10.566%

4.2 The Mechanism of Leading-Edge Vortex Generation

The leading-edge vortex of a propeller is a vortex structure formed at the leading edge of the propeller blade, which has a significant impact on the hydrodynamic performance and cavitation of the propeller. The origin of the leading-edge vortex of a ship's propeller is not always coincident with the tip vortex but typically originates at the inner radius of the propeller blade. The formation of the leading-edge vortex on ship propellers is influenced by the shape and motion state of the fluid at the blade's leading edge. When the propeller rotates, the fluid separates at the leading edge of the blade, creating a low-pressure zone that continually moves and sheds, forming a rotating fluid structure known as the leading-edge vortex

4.3 The Leading-Edge Vortex Correction Model

The leading-edge vortex of a propeller blade is not generated under all operating conditions of the propeller. When the propeller's advance ratio is relatively high, leading-edge vortices are not formed. Only when the propeller's advance ratio is relatively low does the propeller produce leading-edge vortices. This is due to an increase in positive pressure gradient on the blade surface, which leads to flow separation on the propeller's surface. The determination of the threshold positive pressure gradient on the blade surface for flow separation can be made using Equation 16 as proposed by Krüger et al (2019).

$$\frac{dC_p}{ds} > \frac{0.75}{(\log R_n - 2)^2} \cdot \frac{k_1}{D} \tag{16}$$

where dC_p/ds is the gradient of the surface pressure distribution of the propeller, s is the surface length on the blade. $0.75k_1/[D(\log R_n - 2)^2]$ is an empirical threshold value being related to Reynolds number and propeller dimension to predict the leading-edge vortices. R_n is the local Reynolds number. k_1 is a coefficient, and in this work k_1=100000.

The surface pressure distribution obtained from the RANS method in Figure 7 shows that when leading-edge vortices are generated, there is a region approaching the leading edge where the pressure tends to remain relatively constant, resulting in a step-like shape in the surface

pressure distribution. In contrast, the surface pressure distribution obtained from the panel method in Figure 7 shows a continuous increase in surface pressure from the leading edge, without the step-like shape observed in the RANS results. This discrepancy between the panel method's results and the actual propeller behavior can be attributed to the panel method's failure to account for the presence of leading-edge vortices in propeller simulations. Leading-edge vortices on a propeller blade do not form at every location along the cross-section of the blade. As shown in Figure 7, leading-edge vortices occur only when the position along the chord length (x/c) falls within the range characterized by the step-like shape. The correction model for leading-edge vortices primarily addresses this specific range. To determine the extent of this range, this study incorporates Equation 17 proposed by Krüger et al (2019).

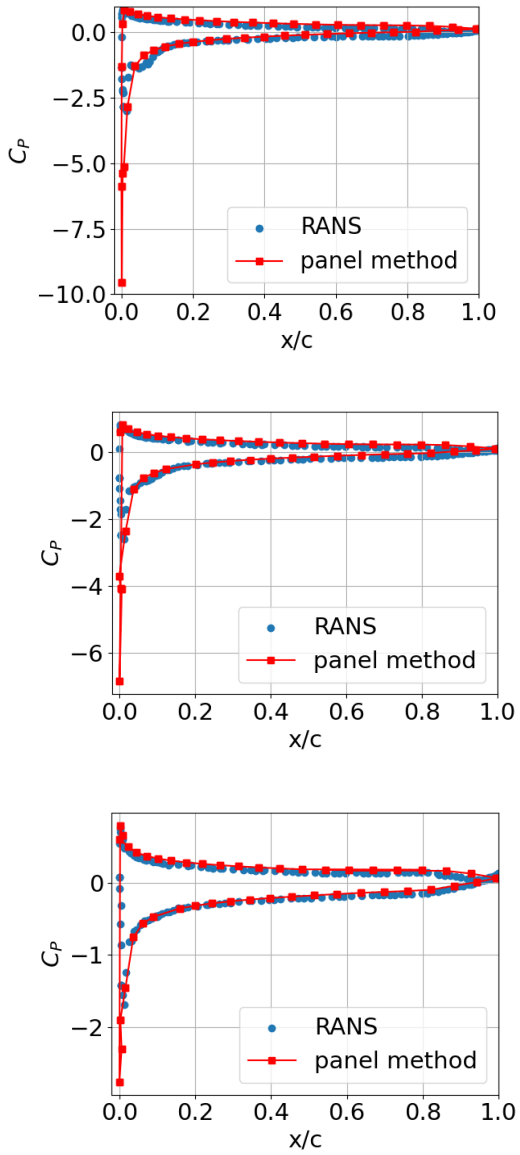

Figure 7 Performance calculation results of propeller in open water at advance ratios of 0.267, 0.4006, and 0.6676

Addressing the fact that the leading-edge vortex originates within the inner radius of the propeller blade and the vortex size increases as it flows to the propeller tip, the leading-edge vortex size along a section at a certain radius r of the propeller is expressed using equation (17), which is in accordance with Krüger et al (2019)

$$l_{sep} = k_2 D \cdot \exp(k_3 \frac{r - r_0}{R}) \quad (17)$$

where l_{sep} represents the size of the leading-edge vortex at a certain radius r. k_2 and k_3 are pending coefficients, where k_2=0.0006, k_3=11.49. r0 represents the minimum radius at which the propeller generates the leading-edge vortex. In order to align the corrected panel method with the surface pressure distribution obtained from the RANS method, the correction model transforms the pressure distribution in the region near the leading edge into a step-like shape. This means that within a specific range near the leading edge, the pressure is maintained at a constant value. Based on the knowledge of the range where the leading-edge vortex occurs, the numerical value of the constant pressure within the correction model is determined by averaging the surface pressure obtained from the panel method in this specific segment.

4.4 Effects of Leading-Edge Vortex Correction Model

Figure 8 compares the pressure distribution obtained with the leading-edge vortex correction model and the RANS method. By comparing Figure 8 and Figure 7, it is evident that the corrected simulation results outperform the uncorrected ones. It is evident that the simulation results with correction outperform those without correction. The corrected panel method program predicts the propeller's performance more accurately and correlates well with the results from the RANS method. This demonstrates the positive impact of introducing the leading-edge vortex correction model in enhancing the accuracy of the panel method simulation.

Table 4 Comparison of calculations before and after leading edge vortex correction model

J	K_T Relative Error		$10K_Q$ Relative Error	
	w/ correction	w/o correction	w/ correction	w/o correction
0.2670	-1.71%	-10.15%	-0.96%	-23.93%
0.4006	-2.71%	-9.16%	-0.48%	-18.62%
0.6676	-4.51%	-7.42%	-2.88%	-10.50%
0.7985	-4.39%	-5.78%	-3.68%	-6.64%
1.0683	-3.90%	-3.90%	-1.82%	-1.82%

Further analysis of the results in Table 4 reveals that the correction effect becomes more pronounced at lower advance ratios. For J=0.267, the relative error of K_T decreases from -10.15% to -1.71%, and the relative error of $10K_Q$ decreases from -23.93% to -0.96%. At J=0.4006, the relative error of K_T decreases from -9.16% to -2.71%, and the relative error of $10K_Q$ decreases from -18.62% to -0.48%. Even at J=0.6676, the relative error of K_T is reduced from -7.41% to -4.51%, and the error of $10K_Q$ drops from -10.50% to -2.88%. The corrected program provides more accurate performance indicators for the VP1304 propeller, with smaller errors and higher precision. This further validates the effectiveness of the leading-edge vortex correction model in improving the accuracy of the panel method simulation.

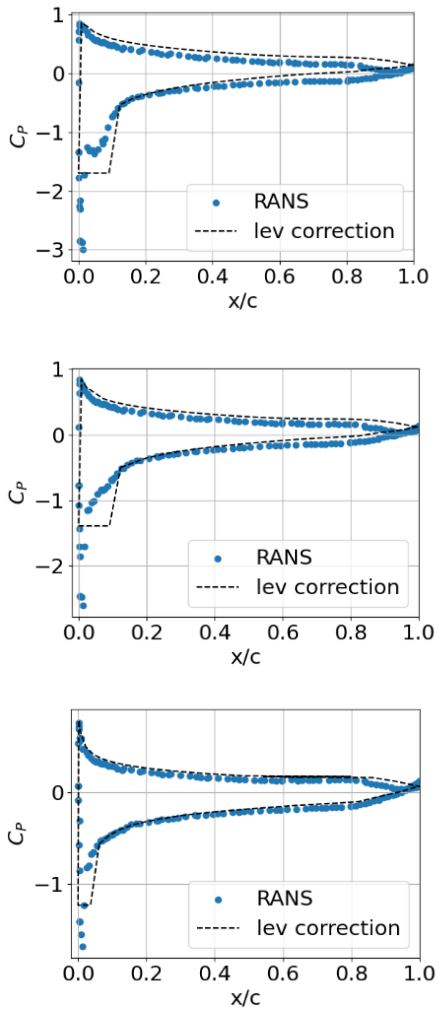

Figure 8 Data comparison plots for r/R=0.7 at advance ratios of 0.267, 0.4006, and 0.6676

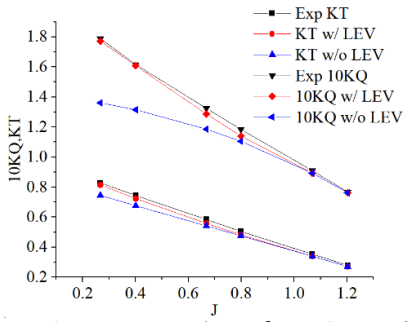

Figure 9 Data comparison of PPTC propeller

4.5 Applicability of the Propeller Leading Edge Vortex Correction Model

To further validate the effectiveness of the leading-edge vortex correction model, this study continued to perform calculations on the P1356 propeller and the E779A propeller at low advance ratios. By comparing the results presented in Table 5, it is evident that the relative error in $10K_Q$ for the P1356 propeller has shown a significant reduction of up to 22.17% following the application of the leading-edge vortex correction model. By comparing the results presented in Table 6, it becomes evident that the relative error in $10K_Q$ for the E779A propeller has shown a substantial reduction of up to 28.14% after the application of the leading-edge vortex correction model. As shown in Table 5 and Table 6, the computed results for various performance metrics pertaining to the P1356 propeller and the E779A propeller exhibit a substantial reduction. This indicates that the leading-edge vortex correction model exhibits good applicability to other propellers as well.

Table 5 Comparison of P1356 propeller data

J	K_T Relative Error		$10K_Q$ Relative Error	
	w/ correction	w/o correction	w/ correction	w/o correction
0.2011	7.65%	-1.00%	6.51%	-15.66%
0.2921	5.96%	-0.18%	2.93%	-11.53%
0.3536	5.12%	0.64%	1.33%	-8.92%
0.4405	3.25%	0.70%	-0.42%	-5.73%
0.5138	1.92%	0.47%	-0.42%	-3.49%

Table 6 Comparison of E779A propeller data

J	K_T Relative Error		$10K_Q$ Relative Error	
	w/ correction	w/o correction	w/ correction	w/o correction
0.199	-1.48%	-8.05%	2.46%	-25.68%
0.249	-1.99%	-8.19%	2.57%	-23.68%
0.298	-2.49%	-7.21%	1.98%	-21.50%
0.348	-3.19%	-7.11%	0.89%	-19.44%
0.397	-4.13%	-7.24%	0.62%	-17.32%

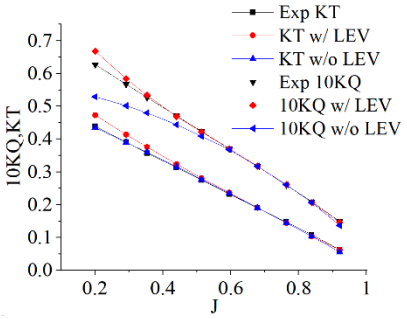

Figure 10 Data comparison of P1356 propeller

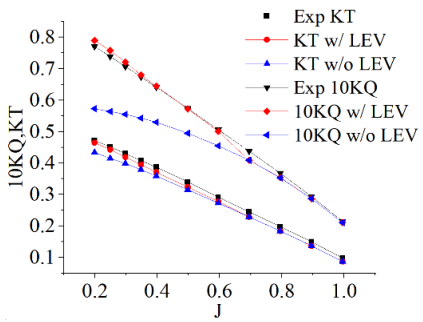

Figure 11 Data comparison of E779A propeller

5 CONCLUSION AND OUTLOOK

This study initially conducted simulations using the SST k-omega turbulence model in STAR-CCM+ to calculate the performance and surface pressure distribution of a propeller. By comparing the surface pressure distribution obtained from the panel method with the leading-edge vortex correction model proposed by Krüger et al (2019), this study found a significant similarity between the two,

further validating the reliability of the correction model. To assess the effectiveness of this leading-edge vortex correction model, it was applied to the calculations of other propellers, followed by comparative analysis. The results demonstrated that the leading-edge vortex model exhibited higher accuracy in predicting propeller hydrodynamic performance. Computational assessments have demonstrated the model's effectiveness in considerably mitigating torque calculation errors.

Due to time constraints, surface pressure distribution for the P1356 propeller and E779A propeller have not been compared with RANS simulations. In the future, we would carry out more validations against more propellers, and a systematic study of the optimal values of the empirical constants in the model.

ACKNOWLEDGEMENT

This work is supported by National Natural Science Foundation of China (Grant No. 52301377), Natural Science Foundation of Shanghai (Grant No. 23ZR1433800), and the Fundamental Research Funds for the Central Universities. The authors are grateful for these supports.

REFERENCES

Barkmann, U., Potsdam Propeller Test Case (PPTC) - Open Water Tests with the Model Propeller VP1304, Report 3752, SchiffbauVersuchsanstalt Potsdam, April 2011

Hess, J. L. & Smith, A. M. O. (1964). 'Calculation of nonlifting potential flow about arbitrary three-dimensional bodies'. Journal of ship research, 8**:**22-44.

Ivashchenko, E. I., Ivashchenko, V. A., Plokhikh, I. A., Mardanov, A. R., Melemchuk, I. A., Pimenov, N. K., & Mullyadzhanov, R. I. (2023). 'Parametric RANS Simulation of a Cavitation Flow in the Channel of a Control Valve Cage'. Journal of Applied and Industrial Mathematics, 17(1):86-93

Krüger, S., Wang, Y., Scharf, M. & Abdel-Maksoud, M.(2019).'A hybrid calculation concept for single and multi-component propulsors'. SMP'19, Rome, Italy.

Lee, C. H. (1988). 'Numerical methods for boundary integral equations in wave body interactions'. Massachusetts Institute of Technology.

Majumder, P., & Maity, S. (2023). 'A critical review of different works on marine propellers over the last three decades'. Ships and Offshore Structures. Mechanical Engineering, 18(3):391-413

Mogollon, J. L., Tillero, E., & Peretti, F. (2022). 'Polymer-EOR Worldwide Potential Contribution to Reducing CO2 Emissions'. Second EAGE Workshop on EOR in Latin America.

Morino, L. & Kuo, C. C. (1974). 'Subsonic potential aerodynamics for complex configurations: a general theory'. AIAA journal, 12**:**191-197

Su, Y. & Huang S. (2004). 'prediction of hydrodynamic performance of marine propellers by surface panel method'. Journal of Harbin Engineering University, 1:9-15.

Wang, Y. (2022). 'An easy-to-implement highly efficient algorithm for nonlinear Kutta condition in boundary element method'. Physics of Fluids, 34(12)

Wang, Y., Abdel-Maksoud, M., & Song, B.(2016). 'Convergence of different wake alignment methods in ia panel code for steady-state flows'. Journal of Marine Science & Technology, 21:567-578

Webster, W. C. (1975). 'The flow about arbitrary, three-dimensional smooth bodies'. Journal of ship research, 19:206-218.